CROSSWELL SEISMIC TOMOGRAPHY

Newkirk Borehole Test Facility Case Study

submitted to

Conoco Inc.

Ponca City, OK

STP Volume 3, No. 3

March 1993

Jerry M. Harris

Seismic Tomography Project

Stanford University

with contributions from

Leon Dahlhaus

Institute for Earth Sciences - University of Utrecht

and

Reinaldo Michelena

Seismic Tomography Project - Stanford University

CROSSWELL SEISMIC TOMOGRAPHY

Newkirk Borehole Test Facility

CROSSWELL SEISMIC TOMOGRAPHY
Newkirk Borehole Test Facility

ABSTRACT

Crosswell tomography can be used to reconstruct the velocity distribution between two boreholes from measured traveltimes. In this study, a dataset collected at Conoco's Borehole Test Facility in Newkirk, Oklahoma was processed using the "strings" iterative traveltime inversion method based on raytracing in isotropic media. Anisotropy and the asymmetrical ray coverage were found to cause huge artifacts in the two dimensional tomograms produced by isotropic strings. Nevertheless, a good interpretation of the 2-D velocity tomogram was made with the help of synthetic data. Comparison of the zero offset crosswell traveltimes with the log-derived sonic velocities indicate nearly 25% p-wave anisotropy in several Newkirk formations. The data were subsequently inverted using a 1.5-D algorithm incorporating an elliptical anisotropy model. The final interpretation from both inversions gives 1-D vertical stratification with layers exhibiting significant p-wave anisotropy. This interpretation is consistent with the sonic logs, crosswell data, and available geological information.

INTRODUCTION

The word Tomography is derived from the Greek for "section image." Tomography produces an image of a medium from data derived from line-integrals (i.e. projections) of the parameter to be imaged. In the case of crosswell seismic tomography, the velocity distribution between two boreholes is reconstructed from observed traveltimes. The traveltimes are approximated as integrals of the slowness along modeled raypaths. In the crosswell geometry both source and receivers are placed down boreholes. Both are located close to the zone of interest and below the attenuating near-surface weathering layer; therefore, high frequencies (kHz) can be recorded and a high resolution image can be achieved.

Crosswell seismic tomography has been used successfully in many geological situations ranging from enhanced oil recovery (Justice et al., 1989) to imaging of geological structures in sediments (Harris et al., 1990) and crystalline rock (Bregman et al., 1989). In most of these cases, few problems were caused by velocity anisotropy and the tie between the tomogram and the well-logs was reasonably good. This does not hold true for the Newkirk site described in this paper.

The data were recorded in September 1991 between two wells at Conoco's Borehole Test Facility (CBTF) near Newkirk in Kay County, Oklahoma. The objective of the study was to verify that traveltime tomography could be used to image vertical stratification with large contrasts and possibly identify layers of natural fracturing if shear waves were observed. An unanticipated result was the large degree of P-wave anisotropy found in some beds. This P-wave anisotropy was first identified with artifacts introduced by an inversion algorithm based on isotropic media. The effect was then verified by reprocessing the data assuming a model with transverse isotropy. This report describes the geological setting, data processing, and the interpretation of the tomograms and well logs. The interpretation is done with the help of synthetic models.

SITE DESCRIPTION

The Conoco Borehole Test Facility is located in the north central part of Oklahoma. There are several boreholes on the testsite and for this survey the Conoco 33-5 and Conoco 33-6 were used. There is a complete suite of wireline logs available for interpretation purposes. The geologic setting is sedimentary with mostly horizontally layered sandstones, shales and some limestones. There are no structurally complex features with the possible exception for three sets of subsurface

vertical fractures (Queen and Rizer, 1990): a NE striking set, a ENE striking set and a ESE striking set. This fracturing has no correlation with depth or stratigraphy, but has been shown to cause subtle shear wave anisotropy in VSP data. A map of the site, identifying the wells used in the survey, is shown in FIGURE 1.

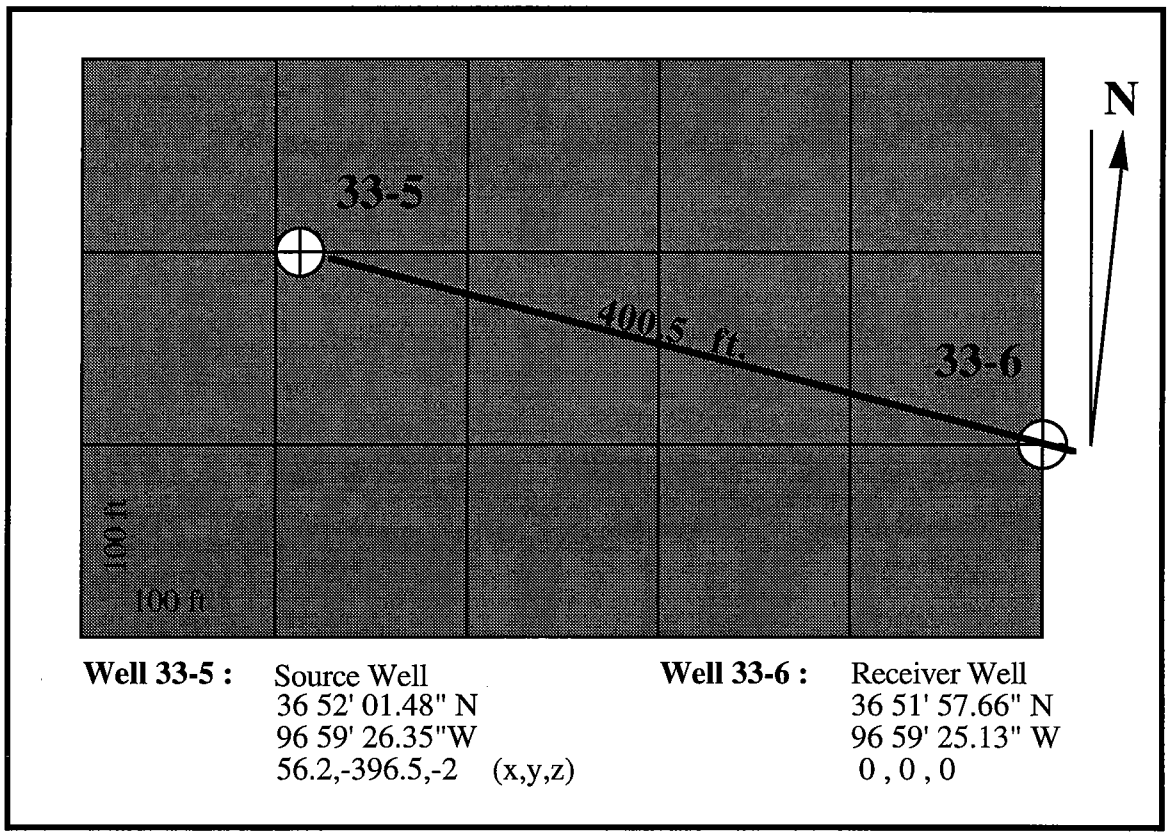

FIGURE 1. Map location of the Conoco 33-5 and 33-6 Wells at the Conoco Borehole Test Facility, Newkirk , Kay County , Oklahoma.

The Conoco 33-5 and Conoco 33-6 well heads are 400.5 feet apart (FIGURE 1) with an azimuth bearing generally ESE. The total deviation with depth of the Conoco 33-5 never exceeds one foot whereas the Conoco 33-6 well is slightly deviated. Surface projections of the 33-6 deviations are plotted versus depth in FIGURE 2, along with the resulting interwell distance to the 33-5. The primary target zone of the tomography lies between depths of 1900 and 2760 feet. The nominal separation of the two boreholes at the target depth is about 404 feet where the well starts deviating in a WNW direction at a depth of 2560 feet. At 2760 feet the well spacing is approximately 384 feet. Nominal borehole diameter is 8.5 inches and there is no casing.

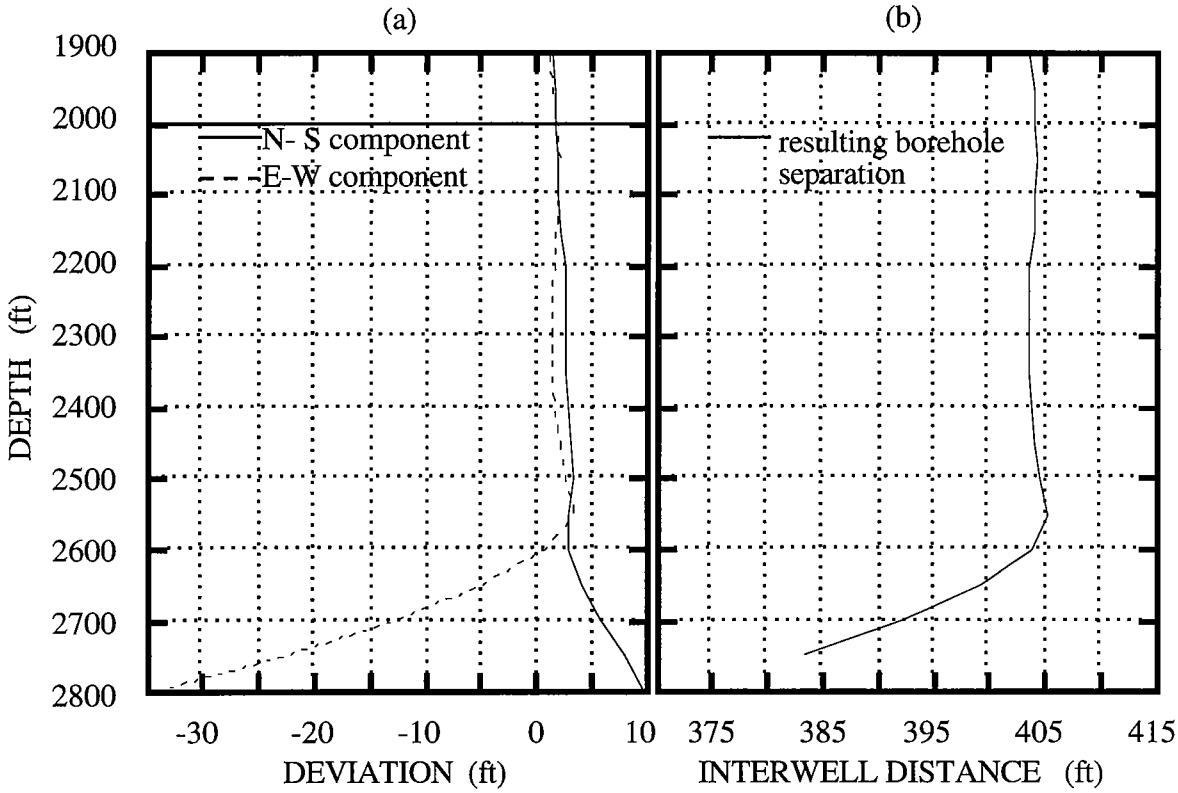

FIGURE 2: (a) Borehole deviation of Conoco 33-6 and (b) the distance between the 33-6 and the 33-5.

DATA ACQUISITION

The field survey was carried out in early September 1991. The Conoco 33-5 was used for the source and the Conoco 33-6 for the receivers. Stanford's two-element, piezoelectric bender was used as the downhole source. The elements were driven in phase for a monopole to generate predominant compressional waves. After initial setup and tests, a sweep signal was chosen with a length of 250.0 ms and start-stop frequencies of 300 Hz and 2400 Hz, respectively. Thirty-two sweeps were stacked to form the recorded seismic trace.

A multi-element hydrophone array was used as receivers, though for different common receiver fans either 6 or 7 elements were used The individual hydrophones, OAS deep ocean models, were spaced 10 feet apart. The data were sampled at 100 microsecond with 4096 samples per trace. A total of 10 common receiver fans were recorded. The typical shooting pattern fixed the receiver array and scanned the source upwards from 2750 to 1900 feet at ten-foot intervals (FIGURE 3). Receiver points covered a depth range from 2760 to 2230 feet also at ten-foot

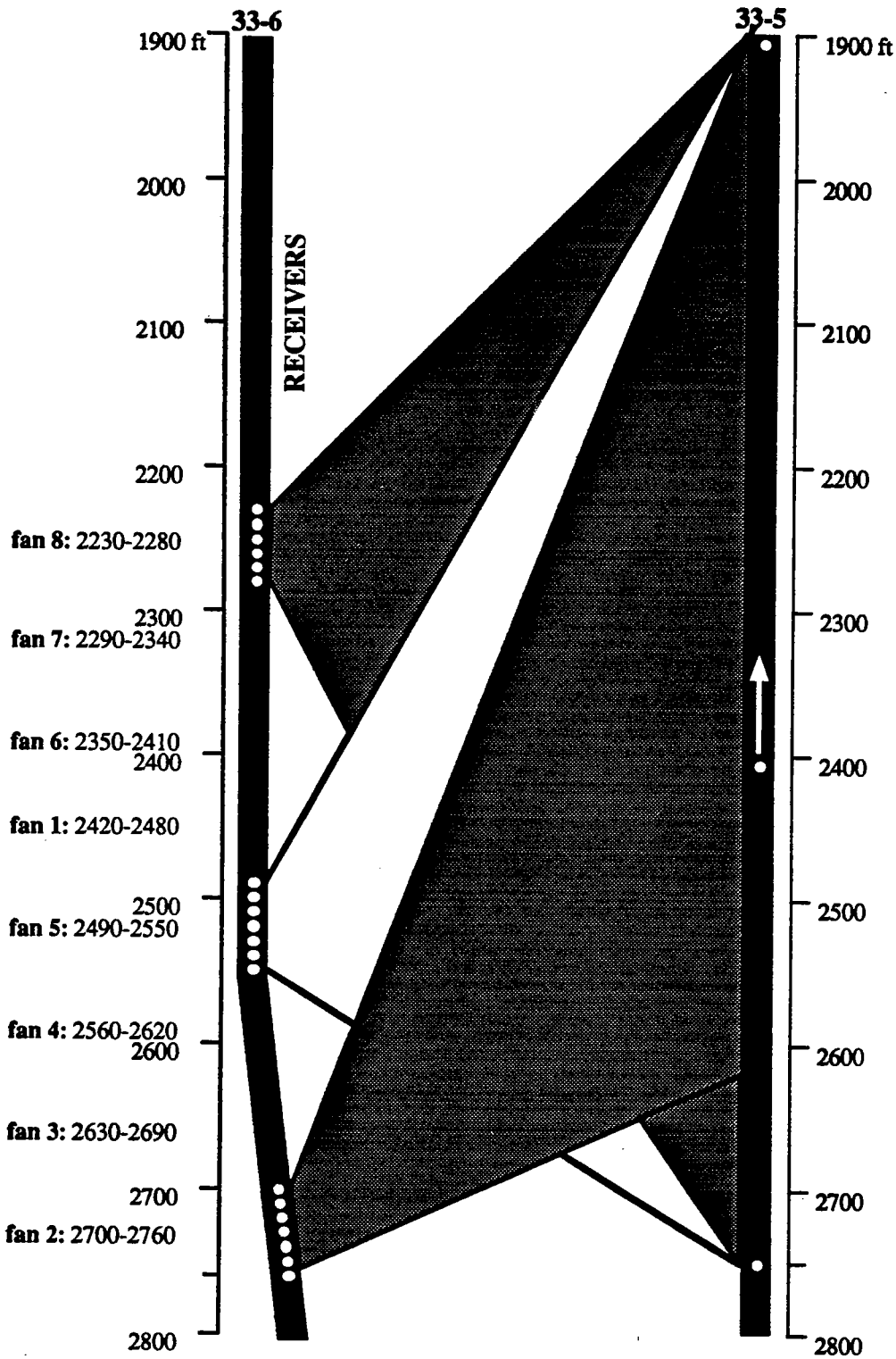

FIGURE 3: Shooting patterns; receiver spacing 10 ft, shot interval 10 ft (fan 1-7) or 5 ft (fan 8).

intervals. Fan 8 (receiver depths 2230 to 2280 feet) was shot at a five-foot source interval by interleaving 10-ft scans. In general, the recording aperture ranged from approximately +65/+10 degrees for the deepest receivers to +40/-50 degrees for the shallowest. Fans 9 and 10 (receiver depths 2475 to 2625 feet) could not be used because of errors in their depth position, probably as a result of mud in the borehole making it difficult to interleave the receiver array between previously recorded depths. The remaining eight fans together provided about 5150 traces of which 4969 were used for traveltime tomography.

DATA PREPARATION AND PICKING

The dataset was edited and picked using ProMAX. During acquisition, a number of traces were repeated because of minor problems with the equipment and readjustment of acquisition parameters. First the raw data were edited and checked for duplicate and bad traces. After removal of these duplicates, the remaining traces were cross-correlated with the pilot sweep. Cross-correlation reduced the record length to 150 ms. Other small recording and geometry problems were then corrected and the dataset completed with blank traces to form a uniform data volume. A typical common-source gather is shown in FIGURE 4. Finally, depth information for the entire survey was written to the trace headers.

Event peaks were picked to extract traveltimes. Picking was done on both common shot gathers (CSGs) and common receiver gathers (CRGs) as well as on common (vertical) offset gathers (COGs). This was done to partly overcome the problem of picking the near offset traces, where it is often difficult to distinguish between direct waves and head waves (FIGURE 5), especially when viewed from only one type of gather. The final result was a set of 4969 gather consistent arrival times. A 2-D chart display of the picked traveltimes is shown in FIGURE 6. This chart also illustrates the recording geometry. A horizontal strip is a common receiver gather; a vertical strip a common source gather; and the diagonals represent common offset and common midpoint gathers. Notice the band of five-feet source-spacing traces and the missing traveltimes, e.g. the big gap for the deepest sources and receivers. In 1-D plane stratified media, the traveltime chart is symmetric about the main diagonal.

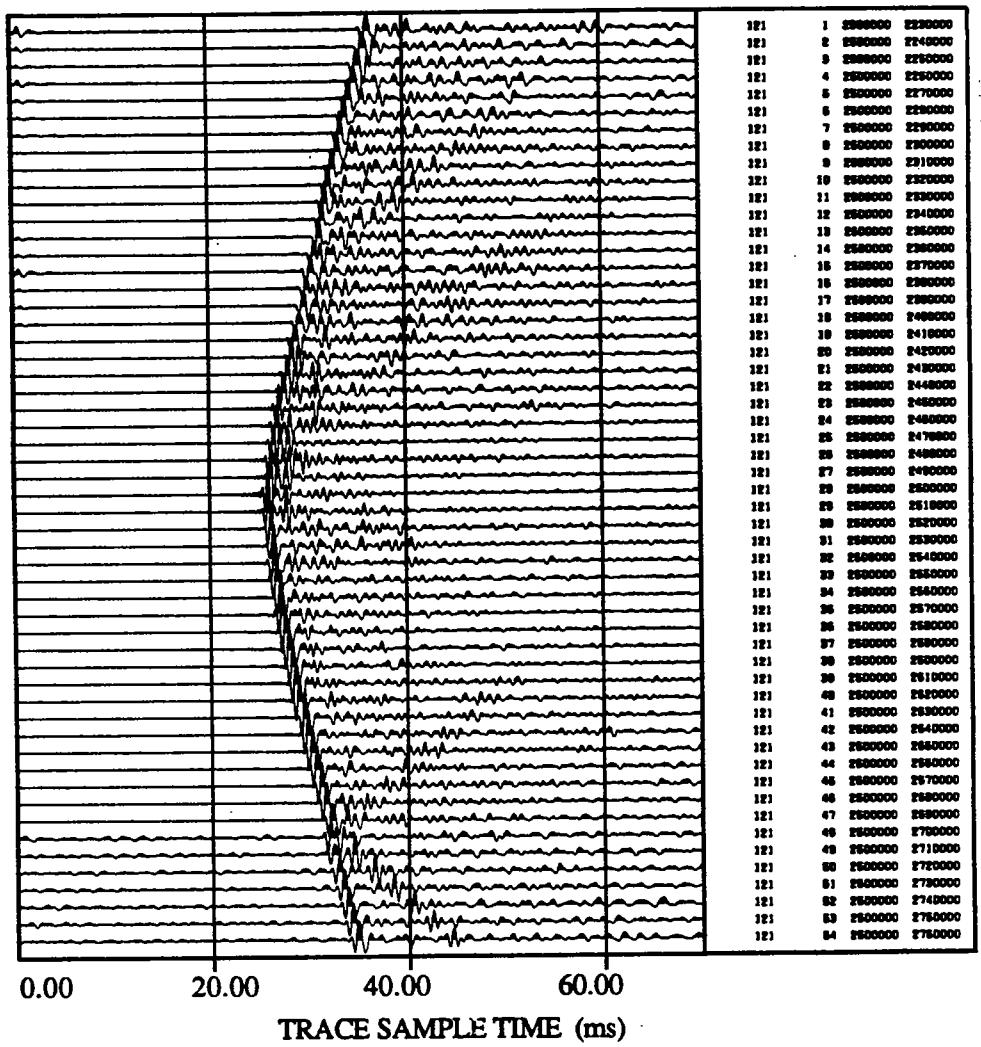

FIGURE 4: Common shot gather at shot depth 2500 ft. The four columns contain respectively source #, receiver #, source depth (in mft) and receiver depth (in mft).

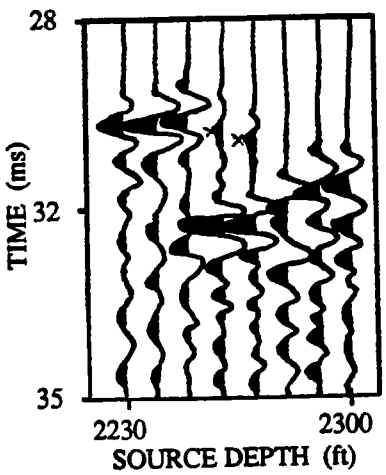

FIGURE 5: An example of picking problems in the near offset traces. In this common receiver gather one should not pick the 'x ' marked headwave arrivals, even though this is the first arriving energy. Instead the fat peaks are the arrivals of the direct waves. A mistake here results in a time error of two milliseconds.and can seriously affect the inversion results.

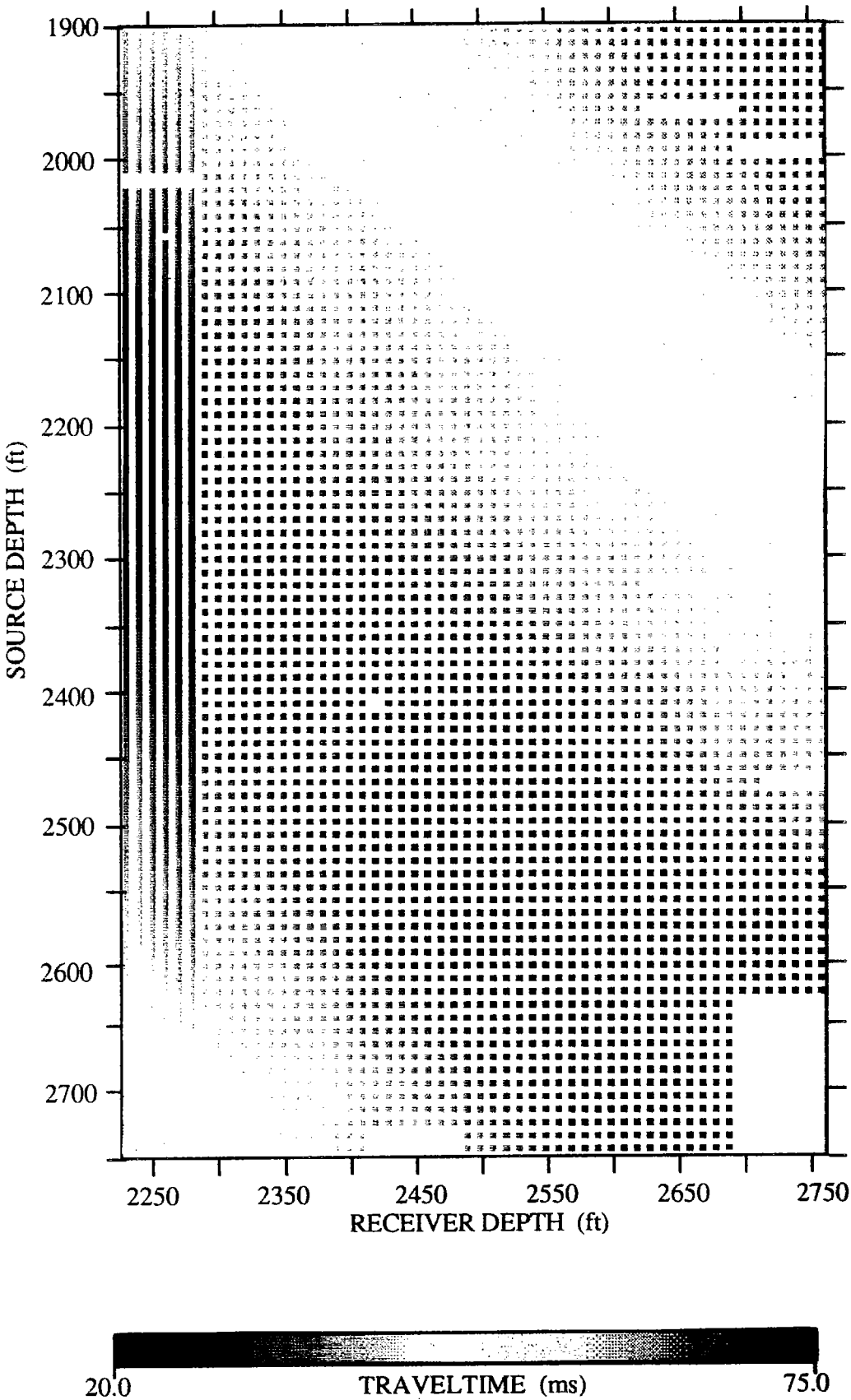

FIGURE 6: Data chart of picked traveltimes: The white stripes and blocks are missing data.

TRAVELTIME TOMOGRAPHY

The picked traveltimes are inverted to solve for the interwell distribution of slowness (inverse velocity). Traveltime inversion in strongly refracting media is a non-linear problem. One has to find both the slowness and the raypaths. One way to do this is to use iterative curved ray inversion such the string algorithm (Harris, 1991). First a raypath is assumed, then a traveltime is calculated by integrating the slowness along the known raypaths. The calculated traveltime is compared to the measured traveltime and a residual is generated. A linear inversion is then performed on the set of residuals. The string inversion algorithm uses the raypaths, contrary to square pixels, as basis functions for the reconstruction of the slowness. The method can be divided in three separate steps (FIGURE 7):

A) Calculate traveltimes τ_i and raypaths for an initial slowness model S_o:

$$\tau_i = \int_C S_o(x,z)\, dl \qquad 1 \le i \le M \qquad (1)$$

To find the raypaths the eikonal equation is solved as an initial-value problem by a Runge-Kutta integration scheme. A dense fan of rays is launched from source points in the direction of the receiver borehole. Pseudo-receivers are placed at points where the synthetic rays cross the receiver borehole. Next, a discrete wavefront is fit to the measured traveltimes. This wavefront is interpolated to produce "observed" traveltimes at the pseudo-receiver positions. This procedure eliminates linking specific source to receiver points, thus speeding up the raytrace algorithm.

B) Backproject the weighted residual traveltime (measured - calculated) along the raypath:

$$\delta S_i = (t_i - \tau_i) / L_i \qquad \text{where } L_i \text{ is the length of the } \underline{\text{ith}} \text{ raypath.} \qquad (2)$$

C) Update the slowness field with a SIRT average, then go back to (A):

$$S^{(k+1)} = S^{(k)} + \delta S^{(k)} \qquad (3a)$$

where

$$\delta S^{(k)} = M^{-1} \sum_{i=1}^{M} (\delta S_i) \qquad (3b)$$

and M is the number of rays influenced by the cell at (x,z). The slowness corrections are added to the initial slowness model (Eqn. 3a) and moved from ray coordinates onto an equi-spaced Cartesian grid. Several backprojections may be run before the raypaths are updated. By definition, an iteration involves only one raytrace regardless of the number of backprojections. Iterations are repeated until an acceptable match between measured and calculated traveltimes is obtained. The string algorithm uses the mean absolute error E_{ma} to track convergence:

$$E_{ma} = N^{-1}\sum_{i=1}^{N}|\delta t_i| \qquad (4)$$

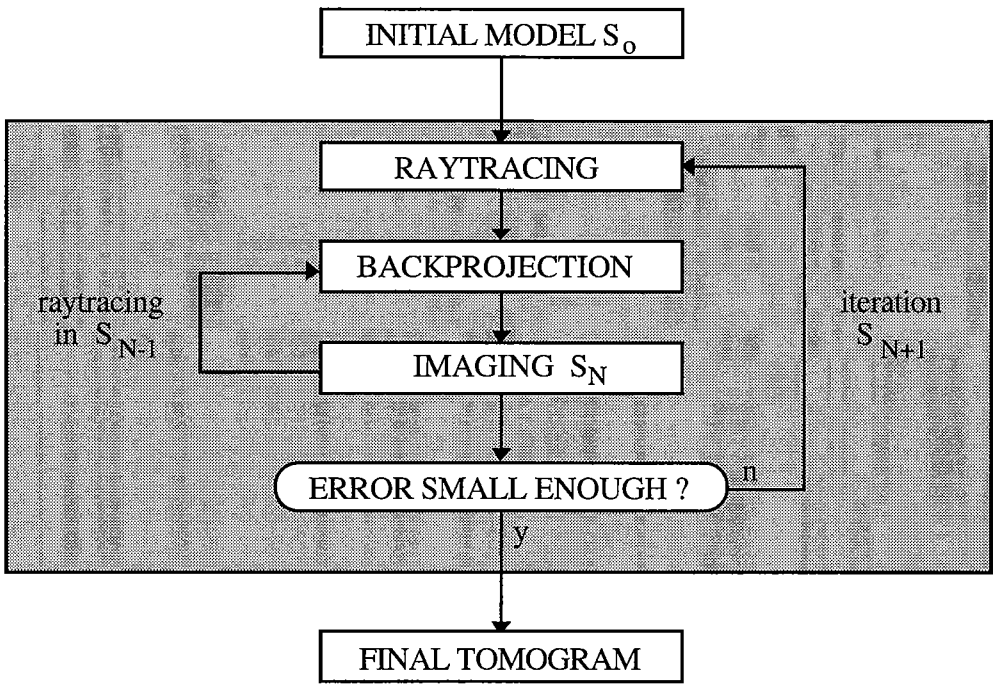

FIGURE 7. Block diagram of the iterative string inversion algorithm.

CBTF FIELD DATA

There are many possible starting models useful in initiating this inversion procedure. However, the linearization step of the algorithm relies on the fact that the actual slowness distribution can be found with relatively small perturbations of a starting model. If the perturbations are too large, it is possible that the procedure converges to an incorrect result or doesn't converge at all. The most common starting models are a constant velocity model and a 1-D layered velocity model. The constant value is best given by the average velocity calculated from all the measured traveltime assuming straight rays. In the case of Newkirk the average velocity calculated from all traveltimes is about 14,000 feet per second. It turns out that variations of a few hundred feet per second do not have a significant influence on the final results. A 1-D model may be derived from the zero-offset traveltimes or from a 1-D inversion initiated by the constant velocity model. The latter gives you homogeneous layers and an estimate of the average velocity as a function of depth.

The layers in the CBTF area are flat-lying. This can be seen by looking at the good correlation of the two wireline logs (FIGURE 18). Therefore it is reasonable to run a 1-D inversion. FIGURE 8 shows the 1-D tomogram of compressional wave velocities after 1 iteration with a constant velocity (14200 ft/s) starting model. The 1-D inversion is accomplished by setting the pixel width equal to the well spacing in the string algorithm. This 1-D structure roughly corresponds to the stratigraphy at Newkirk as can be seen by comparing it with the wireline logs in FIGURE 18. However, the velocities from the tomogram do not match very well the velocities determined from the sonic logs.

The 1-D tomogram is useful for starting the 2-D inversion. Using the 1-D tomogram (FIGURE 8) as a new starting model, a 2-D inversion was initiated. The result after five iterations is shown in FIGURE 9. Parts of the 2-D image with no ray coverage still have the 1-D starting velocity. To compare the effect of the starting model, we also ran a 2-D inversion from a constant velocity start. This result is shown in FIGURE 10. This 2-D tomogram is not much different from the one started with the 1-D model . Both 2-D results are very sensitive to ray coverage; therefore, it is not impossible to assign any geological significance to the lateral variations. In fact, it is clear that much of the 2-D lateral variations in these tomograms are not geology related but artifacts of the inversion. These artifacts are discussed later with a synthetic example illustrating the effects of coverage, missing data, and anisotropy.

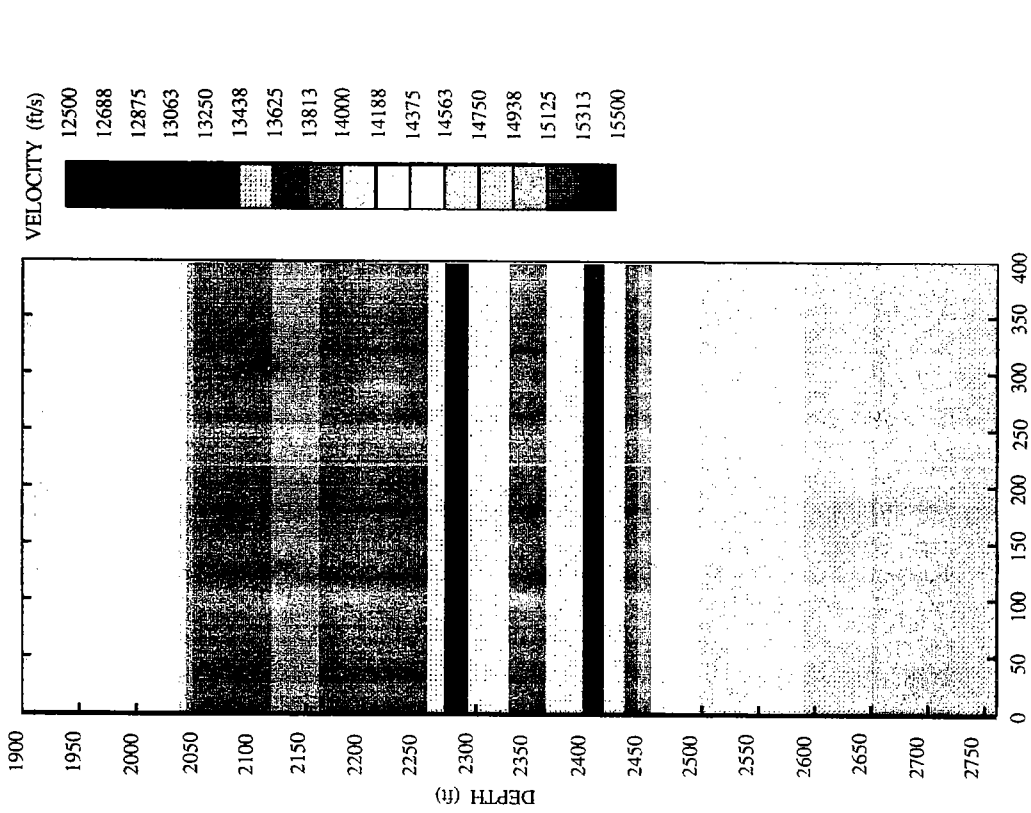

FIGURE 8. 1-D tomogram after 1 iteration: Constant velocity (14200 ft/s) starting model and pixel length in horizontal direction is one time the well-to-well distance.

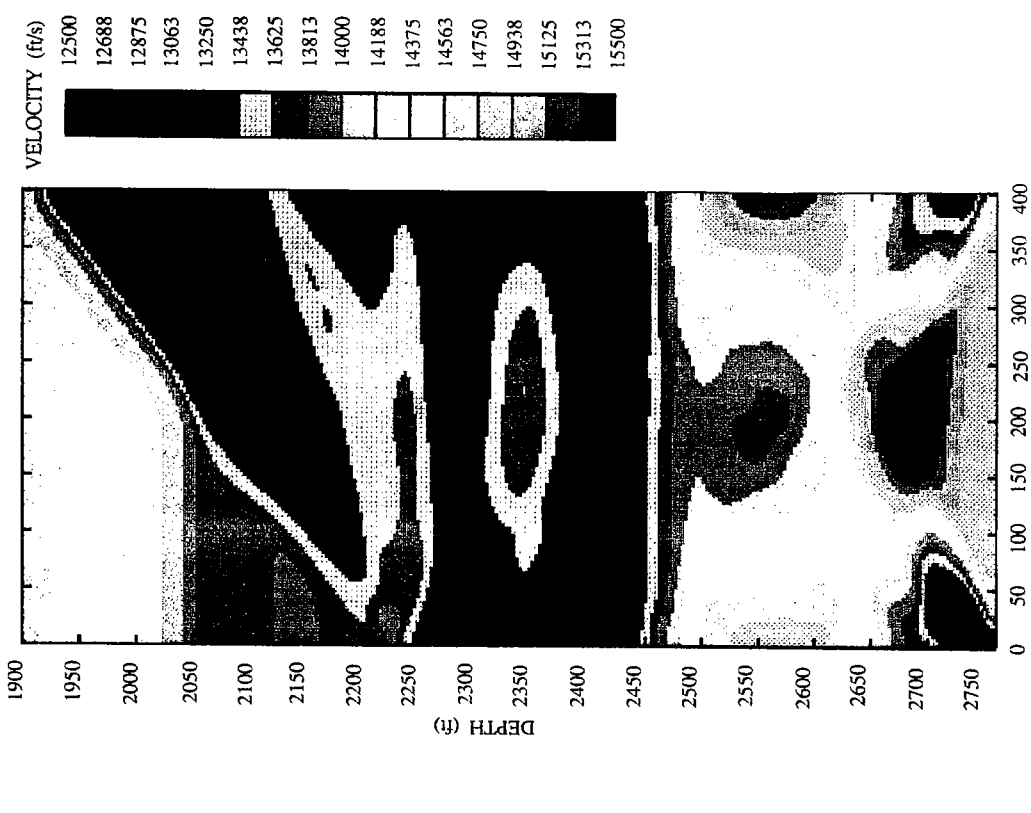

FIGURE 9. 2-D tomogram after 5 iterations: 1-D model (FIGURE 8) used as starting model.

Smoothing

The tomogram in FIGURE 11 clearly shows what happens to the image when no smoothing is applied. Registration of the individual strings onto pixels is visible and the image appears blurred, the result of the simple backprojection. Apart from the aesthetics there are two good reasons for smoothing. First, the inversion model, i.e., strings, cannot easily handle sharp transitions. It is possible that a number of rays could be scattered. The inversion procedure is more stable when there are fewer large discontinuities in the velocity model. Secondly, because of non uniform ray coverage and the discrete string Parameterization there are many pixels with hardly any rays going through. These pixels alone do not influence the inversion. When smoothing is applied, pixels with a lot of rays affect ones with fewer rays, thus rendering the coverage more uniform. However, the smoothing is strictly a post inversion image processing effect; therefore the traveltime residual after smoothing is different than before. In the case of Newkirk, I used a lot of smoothing on the first iterations and gradually less with increasing iterations. The main smoothing is done in the horizontal direction for two reasons: The lack of near vertical rays in this crosswell configuration results in poor lateral resolution. Therefore it is appropriate to smooth in horizontal direction. Also, the strong evidence for horizontal layers in the CBTF site justifies the use of lateral smoothing. Nevertheless, the final iterations are done with very little smoothing.

Well deviation

Well deviation must be considered when it is significant compared to the distance between the wells. The string algorithm uses a ribbon system of coordinates (Harris, 1992). The ribbon is formed by calculating a pointing vector between every shot and receiver pair. Because well deviation is usually gradual, this pointing vector rotates slowly with depth thus forming the ribbon. Within each CRG or CSG the ribbon is practically 2-D and the algorithm, e.g., raytracing and inversion, can work as if it were perfectly 2-D. At Newkirk one of the two boreholes is straight and the other is only slightly deviated in the lowest zone of interest. Comparison of inversion results with and without deviation correction showed only a subtle difference at the bottom part of the tomogram where the deviation occurred.

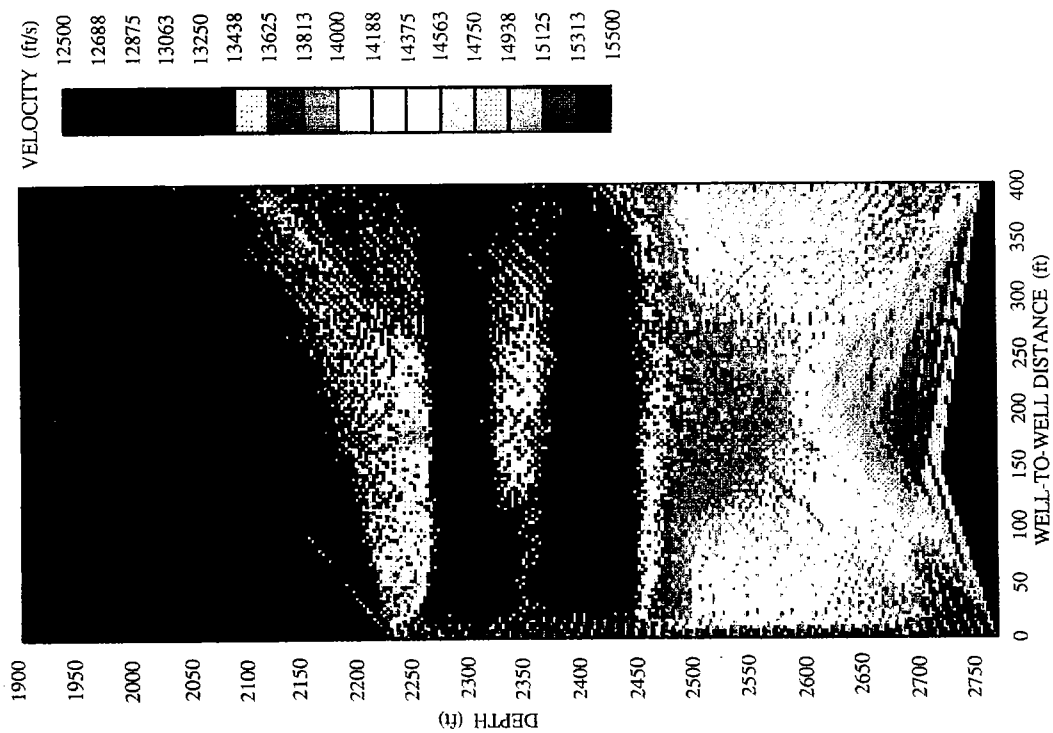

FIGURE 11. Crosswell tomogram after 2 iterations: No smoothing applied.

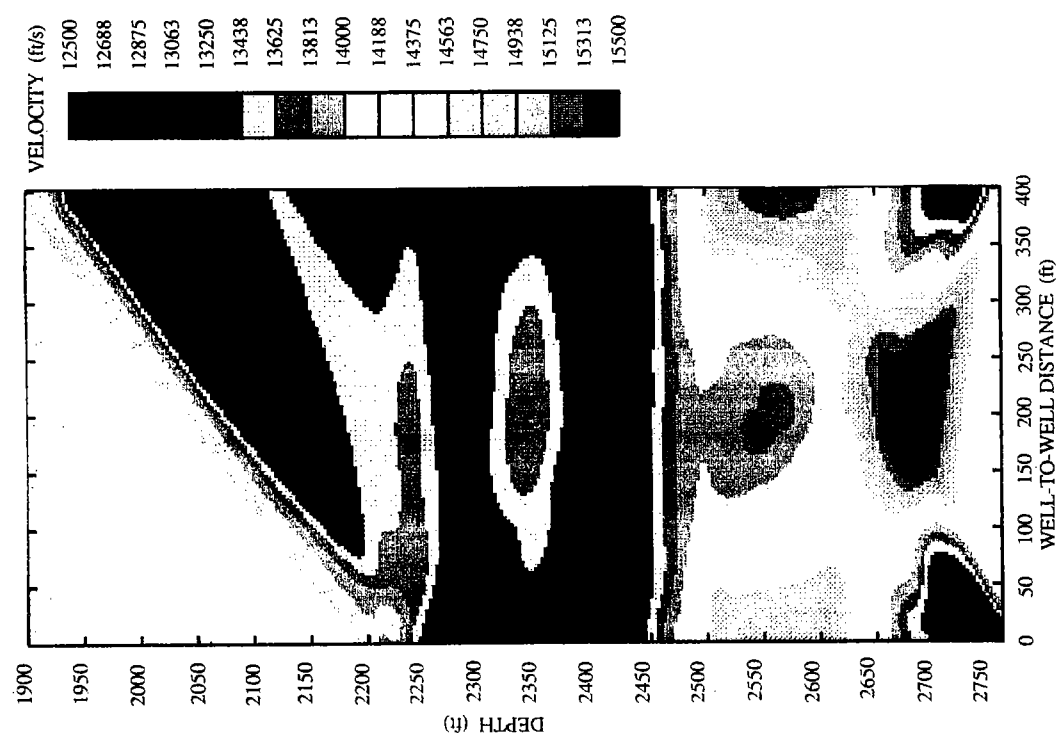

FIGURE 10. 2-D tomogram after 5 iterations: Constant velocity (14200 ft/s) starting model.

Shooting aperture

Not only does the near vertical boreholes of the crosswell geometry limit the angles of the raypaths and thus the resolving power of the experiment, but also the way in which the rays are shot during string inversion has a significant influence on the inversion. This is because the rays are not linked as discussed above. The use of a small aperture around the zero offset depth gives a low resolution 1-D image, because there is hardly any information about lateral variations from more vertically traveling rays. The tomogram in FIGURE 12 is an example of this effect. Remarkable is the fact that the large velocity variations in the depth range 2500-2700 ft are changed into a uniform high velocity zone when using only near horizontal information. All the rays were shot between +/-15 degrees and the result is a laterally smooth image. On the other hand, using only large offset traveltimes will reduce vertical resolution. This is demonstrated in FIGURE 13 where the tomogram was made with rays shot in the aperture +13 to +65 and -13 to -55 degrees. The Newkirk dataset does not have many large angle rays. Based on these findings, the aperture for the final tomographic inversion was selected to be zero to +/-45 degrees.

Coverage - missing data

Gaps in the dataset will produce artifacts in the tomograms also. It is important to distinguish these non geology related features from other information in the tomogram. Looking at the data chart (FIGURE 6), it is clear that there will be problems with missing data and asymmetrical coverage. The large block of missing information from the deepest source - receiver pairs and the absence of receivers from 1900 to 2230 feet depth are responsible for many of the artifacts in the images. In order to get a better feeling for what the effects of the asymmetrical geometry are, we made a symmetrical subset of the data from 2230 feet to 2630 feet. This subset should be sufficient to remove the major artifacts caused by asymmetric coverage. The result is shown in FIGURE 14. This tomogram shows that the velocity distribution in the lower part of the image is much smoother because there are no gaps in the data. Another way of avoiding the problems caused by missing traces would be to interpolate (and extrapolate) the data. FIGURE 15 was produced using the data produced by an extrapolation routine based on fitting hyperbolas to local traveltime curves (Harris and Wang, 1992). Here also the image is much smoother, although the extrapolation part does not have the desired results. This may be caused by the fact that the extrapolation algorithm does create new independent data, but instead gives a smooth estimate outside the field aperture by fitting smooth curves to the measured data.

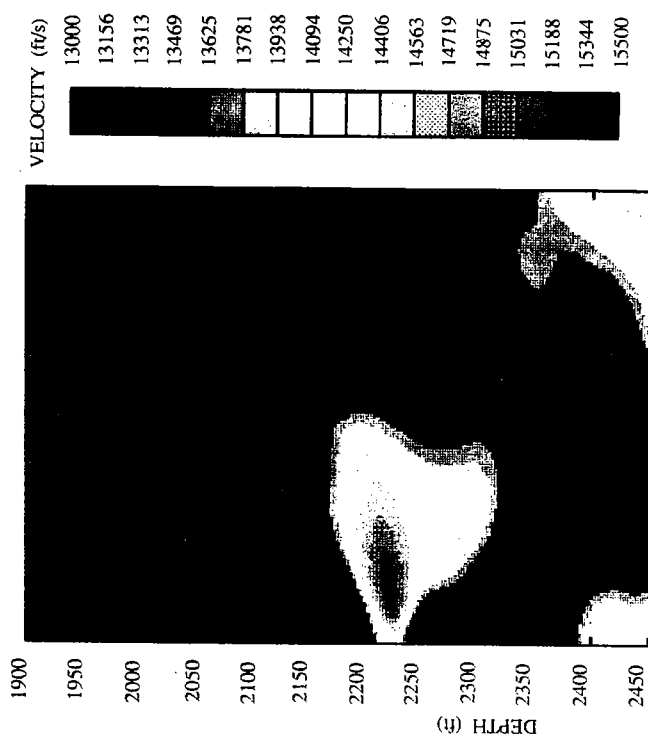

FIGURE 13. Crosswell tomogram using only ray aperture of +13 to +65 and -13 to -55 degrees.

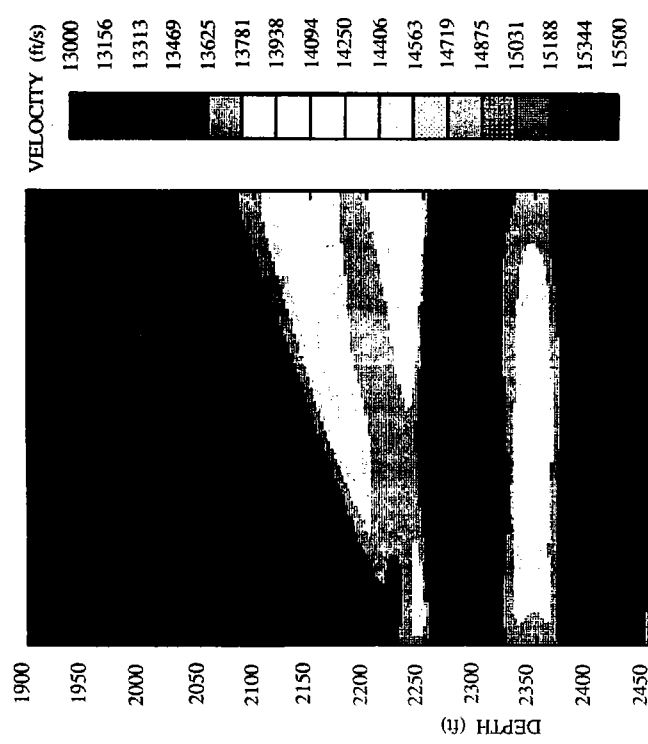

FIGURE 12. Crosswell tomogram using only a ray aperture of plus and minus 15 degrees.

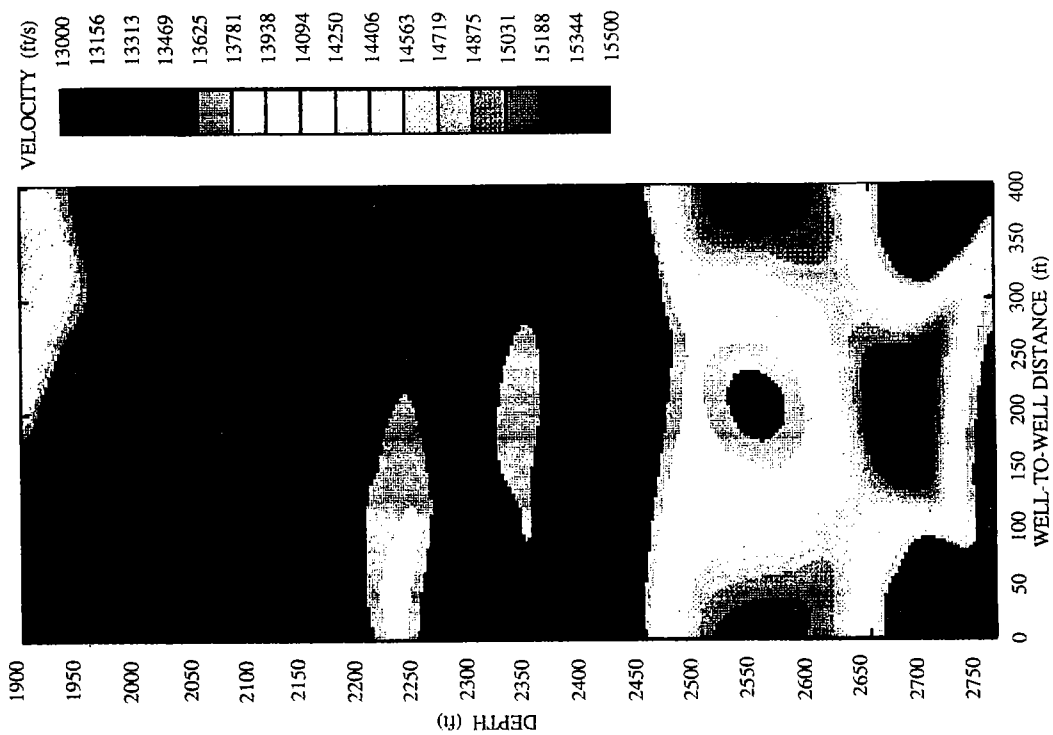

FIGURE 15. Crosswell tomogram of the interpolated and extrapolated dataset.

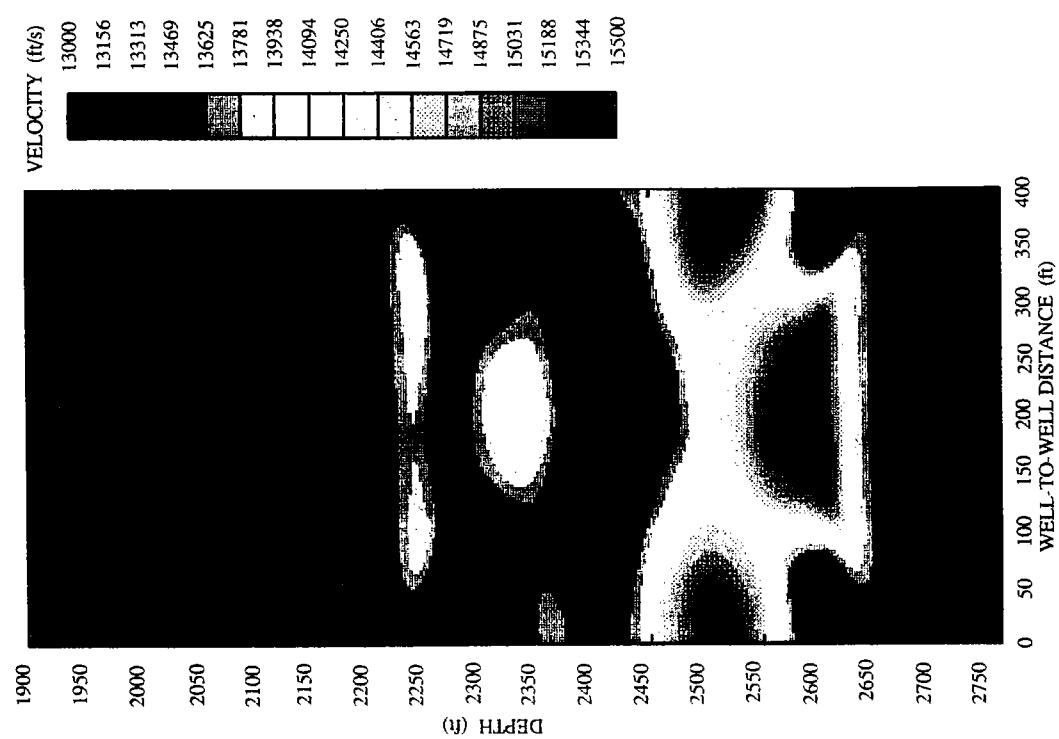

FIGURE 14. Crosswell tomogram from a symmetric subset of the full dataset (2230 - 2630 feet)

Final Isotropic Inversion on Field data

In the previous sections several tomographic images obtained with the isotropic inversion algorithm. The main stratigraphic features of the site can be found in each of the inversions. We'll next make the best tomogram for interpretation. The starting model is a constant velocity model (14200 ft/s). The pixel size of the tomogram is selected to be 3 by 3 feet. Horizontal smoothing is used in the first few iterations and no correction is made for the well deviation. The aperture of shooting the rays is +/-45 degrees. For this inversion, the mean absolute error is plotted for nine iterations in FIGURE 16. The final crosswell P-wave tomogram is shown in FIGURE 17. The tomogram together with the most important wireline logs and mud report are presented in FIGURE 18.

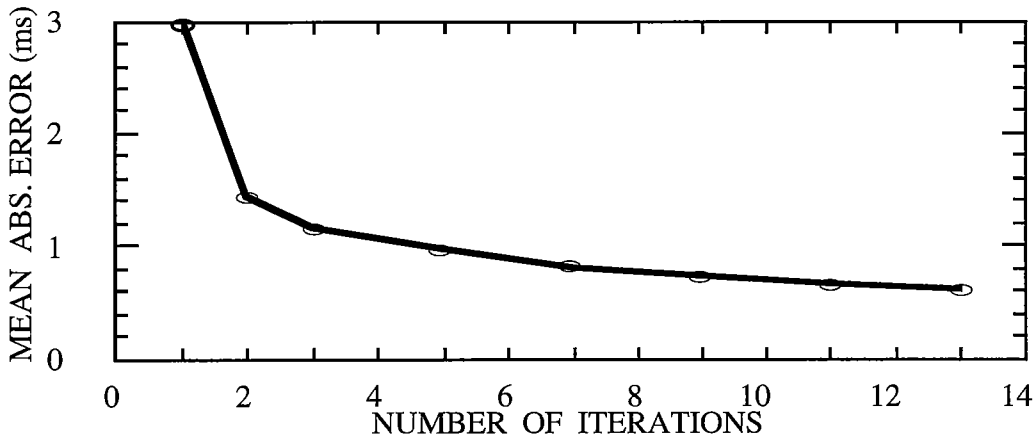

FIGURE 16. Mean absolute error of the iterations of the final Newkirk tomogram.

A first examination of the final tomogram (FIGURE 17) based on the isotropic model clearly shows two poorly imaged areas; the triangular shaped one in the upper left part of the image and the arc-like feature at the bottom. These are due to the asymmetrical coverage and missing data. As a result, only the middle part of the tomogram (2200-2700 ft) can be used for interpretation. Comparison of the tomogram and the (sonic) logs shows poor correlation. We see that only the low velocity sandstone zone at a depth of approximately 2400 ft appears to correlate correctly. What causes the prominent artifacts and mispositionings in the rest of the tomogram?

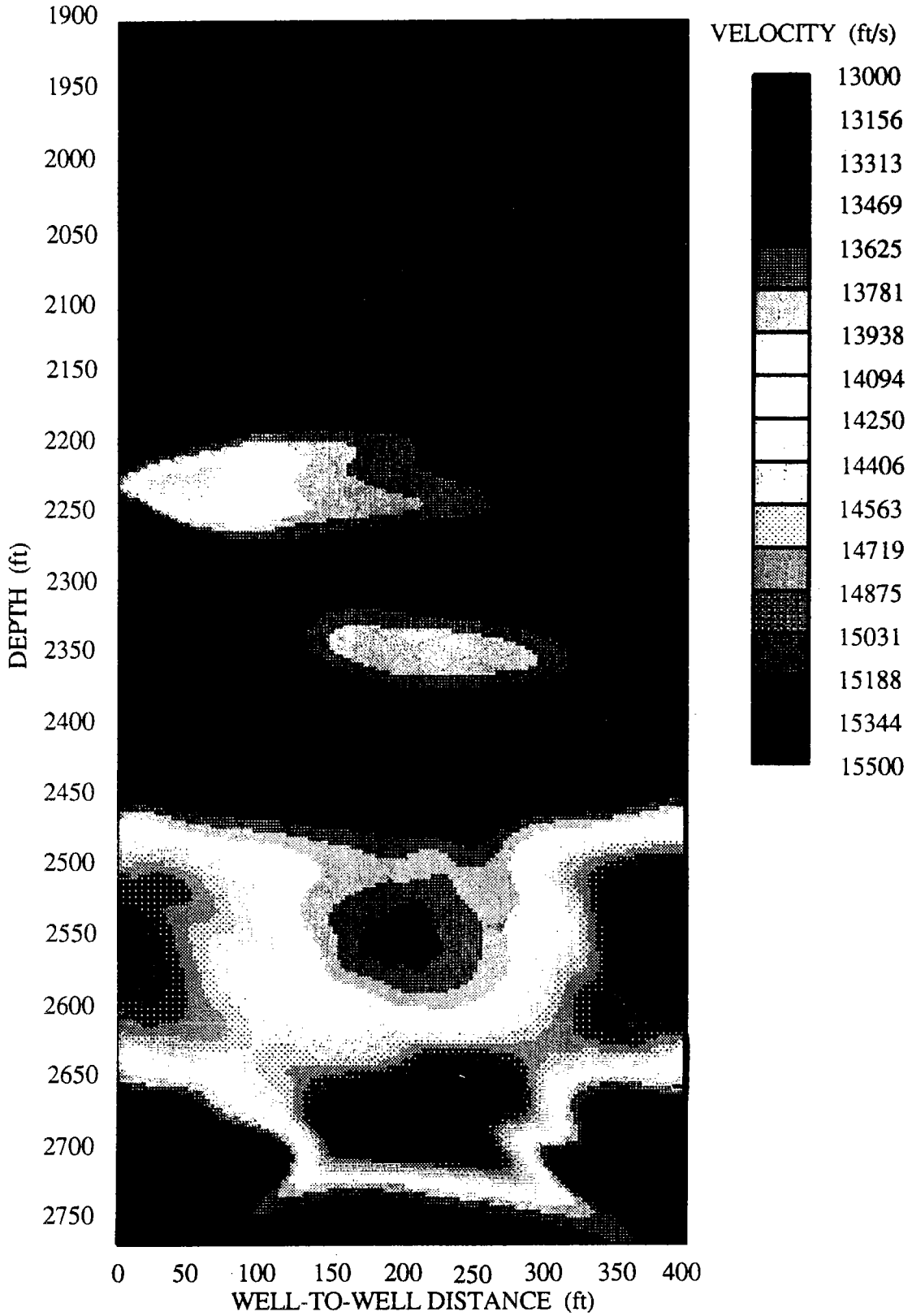

FIGURE 17. Final Newkirk tomogram from isotropic string algorithm.

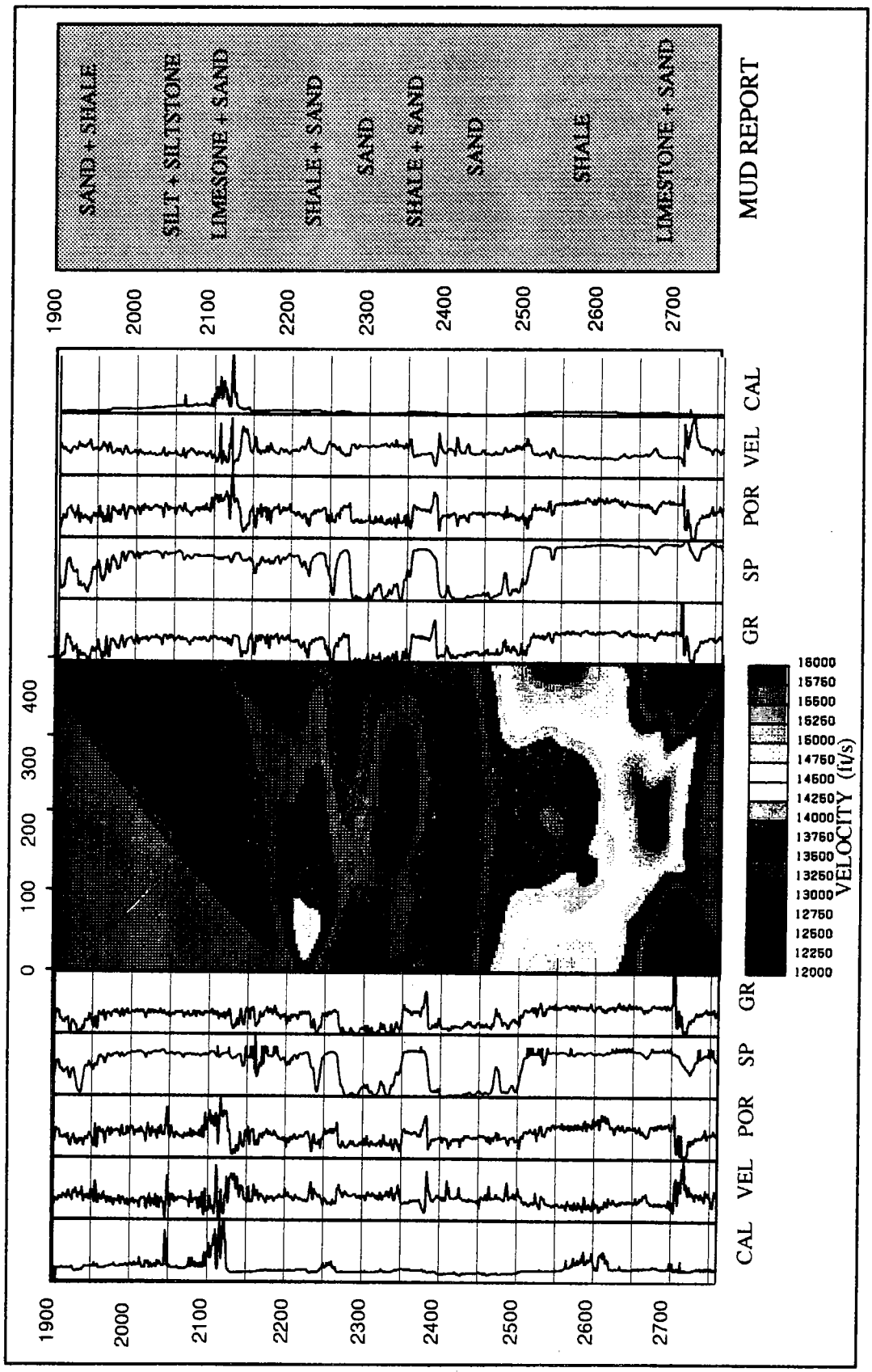

FIGURE 18. Newkirk tomogram with wireline logs.

Part of the answer was given in the previous sections. There we discussed how aperture, missing data, and coverage each can distort the image. However, in real data these factors usually coincide and interfere, thus making the interpretation extremely difficult. Look for example at the difference between FIGURES 14 AND 17. The tomogram in FIGURE 14 was made from a symmetrical subset of the complete dataset. The most remarkable change is that the fan - shaped feature at a depth of 2230 ft now is symmetrical. Also the overall smoothness is increased because there are hardly any holes left in this subset. In both the upper and lower part of the tomogram there are similar velocity distributions. These can not be explained by anything other than non - uniform coverage combined with angle - dependent velocities (discussed below).

ISOTROPIC SYNTHETIC

To test the error hypotheses, we created two synthetic traveltime datasets for inversion, one isotropic, the other anisotropic. The isotropic, synthetic model for this experiment is derived from the zero vertical offset crosswell velocities. A 1D raytracer was used to create the synthetic traveltimes. The same (9 iterations) inversion procedure as for the field data was first applied to the isotropic model, yielding the tomogram shown in FIGURE 19. The velocities are reconstructed very well and only the geometry and coverage problems near the edges cause artifacts. To see the effect of missing data and to make the synthetic inversion more realistic we removed the same traces that were missing in the field data. The resulting tomogram is shown in the FIGURE 20. Notice the un-imaged background velocity zones at the bottom of the images. These are caused by the missing of the deepest source - receiver pairs.

TRANSVERSE ISOTROPY

It is known that P wave anisotropy can occur in laminated shales. In a thick homogeneous section, the zero vertical offset crosswell traces (source and receiver at the same depth, FIGURE 21) can be used to obtain an estimate for the average horizontal velocities between the two wells. This is done using the first arrival times and the correct values for the separation of the boreholes. The sonic logs give a good indication of the vertical velocity. In FIGURE 22 the median filtered sonic velocities at the two wells are compared with the zero offset crosswell velocities. The most striking difference in velocities can be seen at depths between 2500 and 2700 ft. In this interval the average horizontal velocity from the crosswell data is approximately 15000 ft /s and the vertical velocity from the log is about 11500 ft/s. The high values in the SP, Gamma Ray and Calculated Porosity logs as well as the mud reports for this interval indicate a thick shale formation (FIGURE 18).

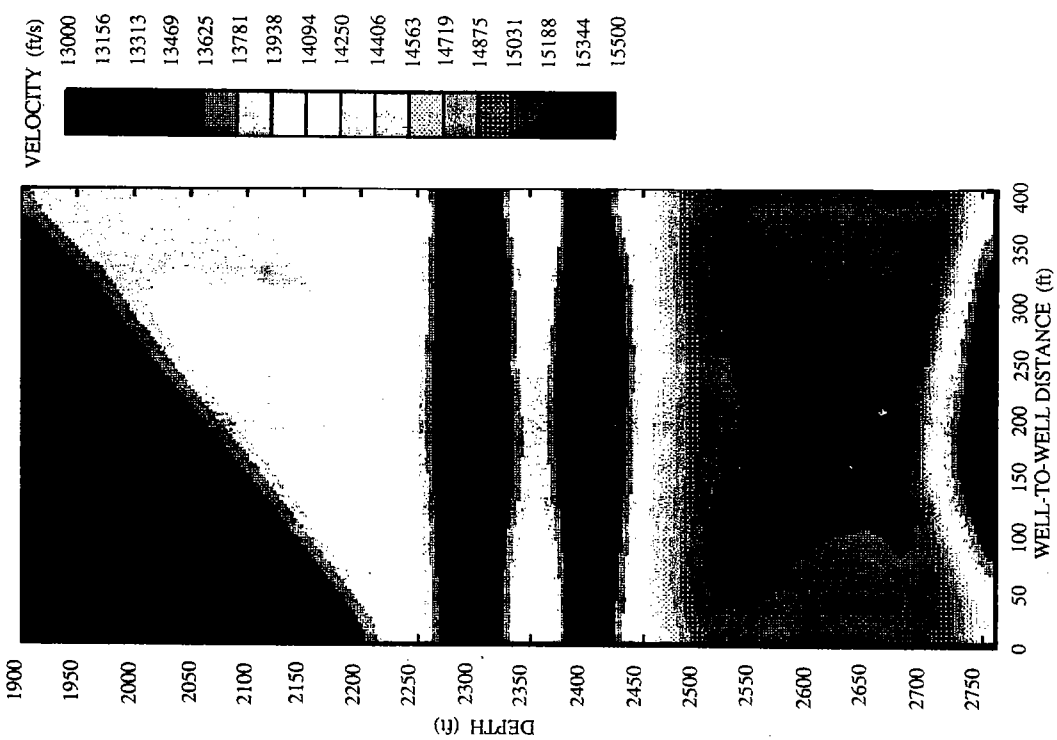

FIGURE 20. Crosswell tomogram: synthetic data (with missing traces) from isotropic model.

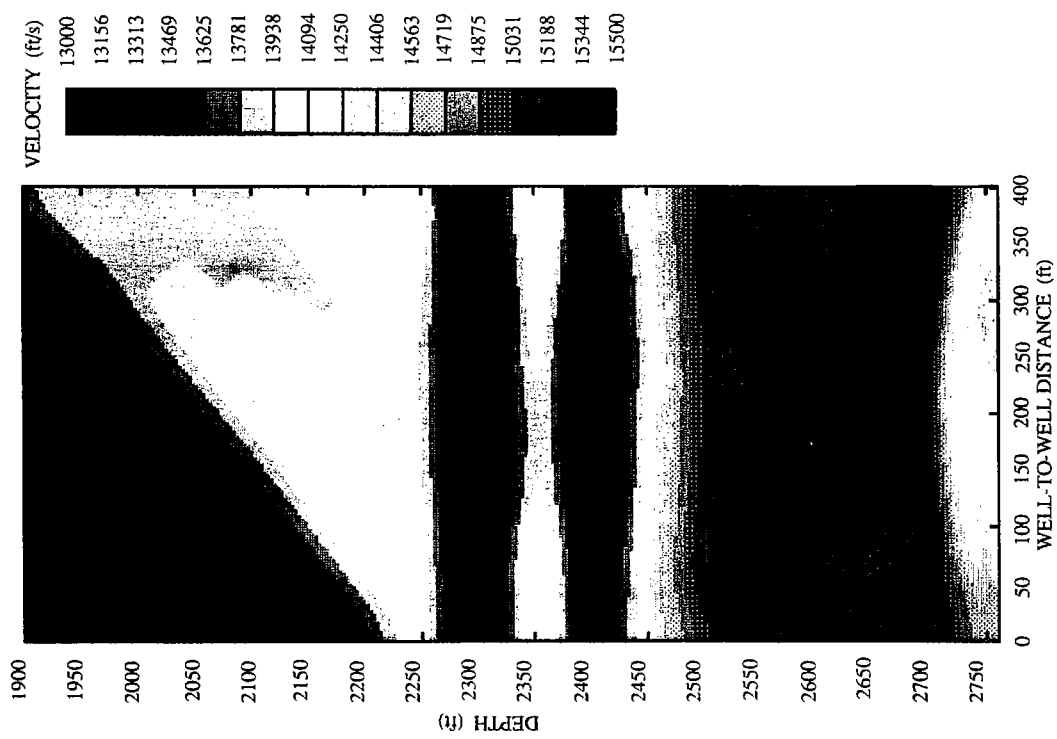

FIGURE 19. Crosswell tomogram: synthetic data from isotropic model.

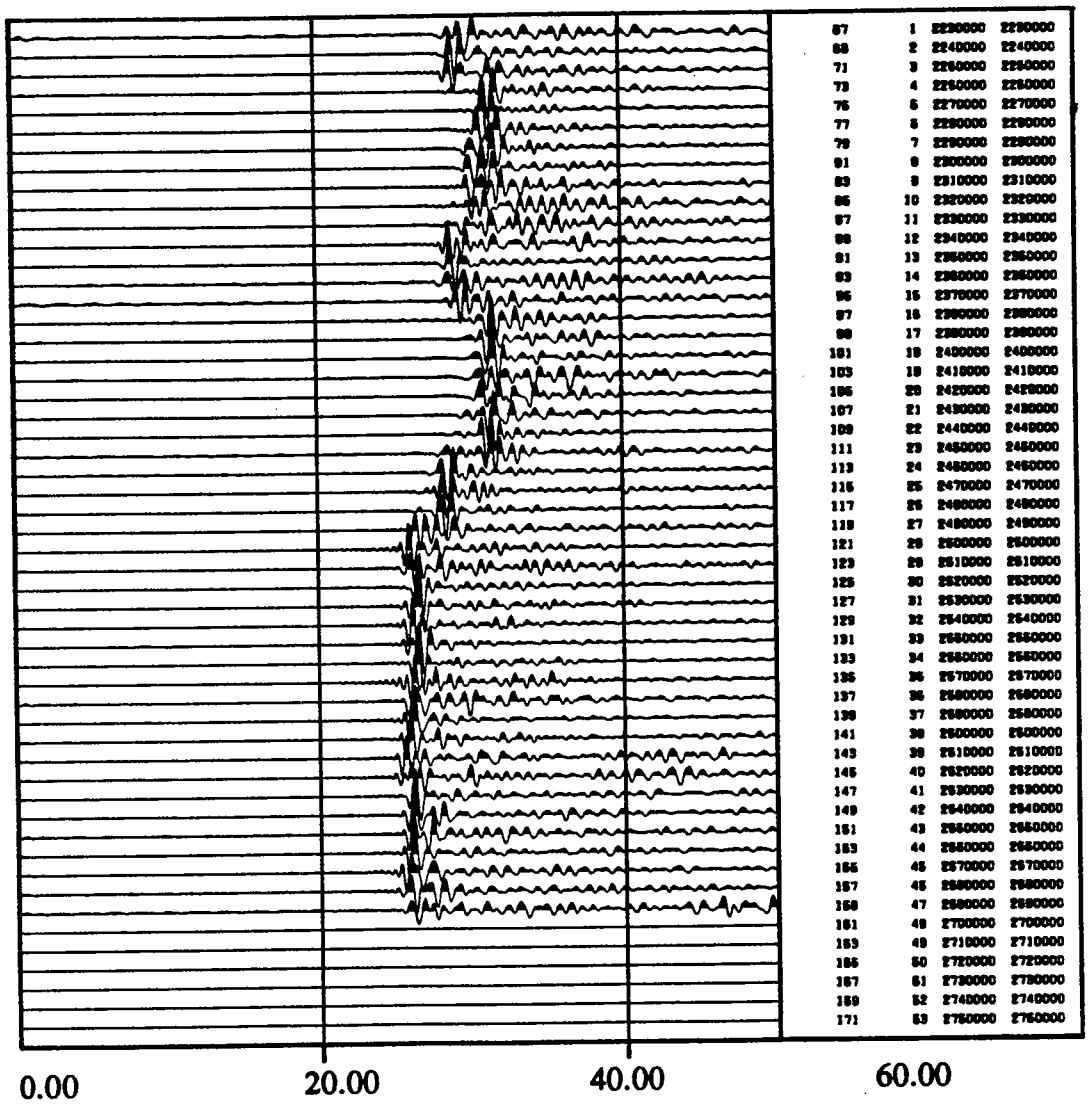

FIGURE 21. Zero vertical offset gather. The four columns contain respectively source-number, receiver-number, source-depth (mft) and receiver-depth (mft).

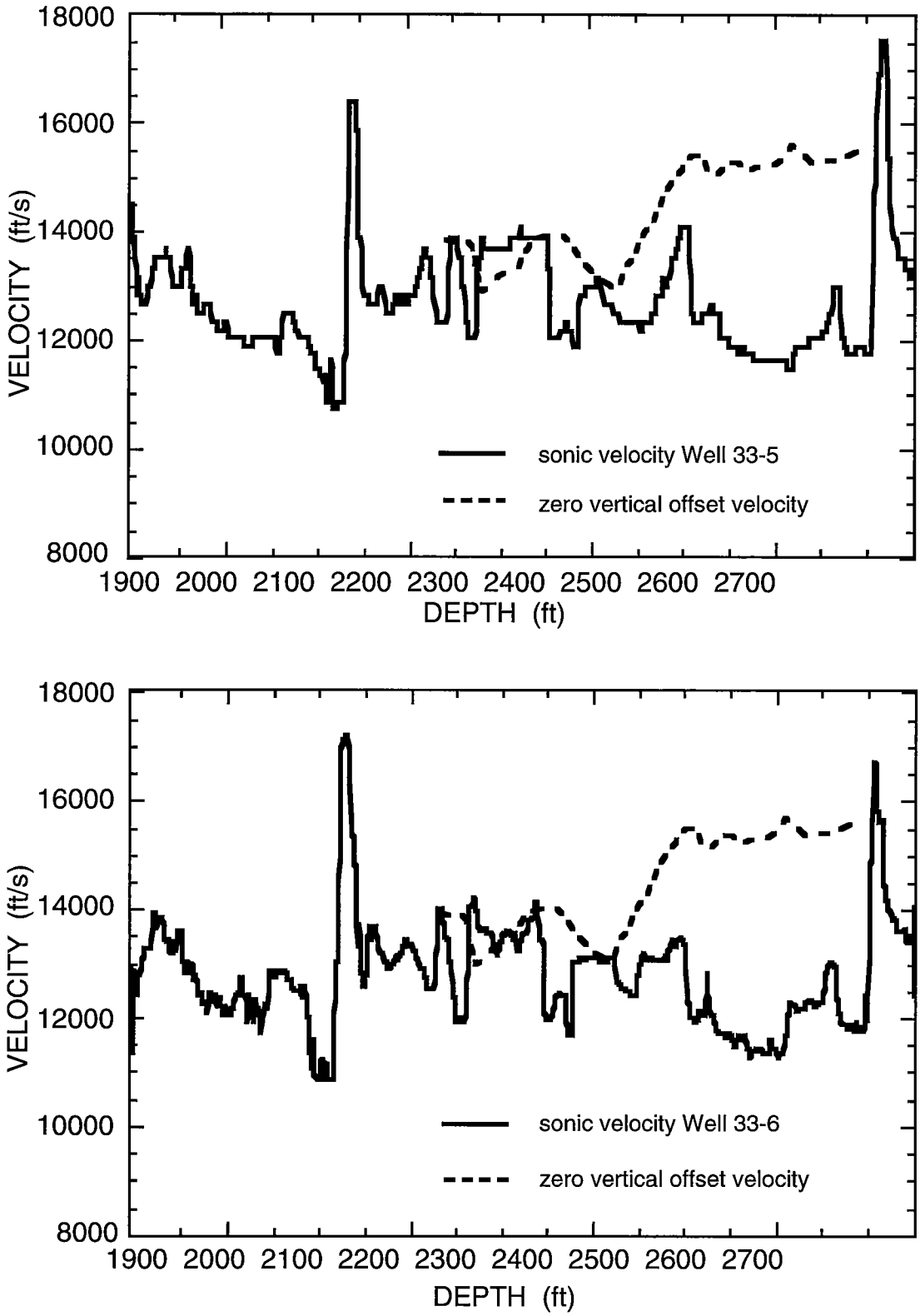

FIGURE 22. Comparison of sonic logs and zero vertical offset velocities of the Newkirk wells.

First, we note that one can obtain a "rough" indication of the amount of anisotropy by running the isotropic inversion using altered well spacing which can be estimated from the following expressions:

$$X = T_1 \, \Delta Z \, (T_2^2 - T_1^2)^{-1/2} \qquad (4)$$

and

$$X = X_0 \, V_z \, V_x^{-1} \qquad (5)$$

where T_1 is the zero vertical offset (horizontal) traveltime, T_2 the traveltime from a source - receiver pair with offset ΔZ, X_0 the actual well-to-well distance and V_X and V_Z the horizontal and vertical velocities for an elliptical velocity model. The results of this calculation for the lower part of the Newkirk isotopic tomogram are given in Table 1. For a homogeneous medium, reducing the well's offset is equivalent to to contracting the vertical component of velocity for an equivalent elliptical anisotropy model. Average values for the horizontal and vertical velocities in the lower part of the image that are found this way are 15500 ft/s and 10500 ft/s.

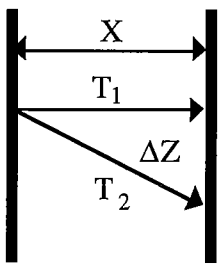

Z_1	Z_2	T_1	T_2	ΔZ	X
2500	2600	25.93	28.33	100	227
2500	2700	25.93	32.03	200	275
2550	2650	26.13	28.16	100	250
2550	2750	26.13	31.46	200	298
2600	2700	25.94	27.25	100	310

Table 1. Parameters chosen for the computation of a pseudo well spacing for an isotropic homogeneous medium emulating an elliptically anisotropic homogenous medium.

TRANSVERSE ISOTROPIC STYTHETIC

To further test the anisotropy hypothesis, we created a synthetic using a 1-D transverse isotropy model and performed the same string inversion (FIGURE 23) again. In order to identify the artifacts related to missing data and asymmetrical coverage, we created a symmetrical subset of the synthetic anisotropic model data and removed the same data missing from the field survey. The inversion results anisotropic synthetic dataset are shown in FIGURE 24 (complete dataset) and FIGURE 25 (missing data). Again, as with the isotropic model, the tomogram is smooth and symmetrical. Comparing the anisotropic synthetic tomogram (FIGURE 25) with the final isotropic inversion result of the field data (FIGURE 17), one sees remarkable similarities, especially in the lower shale section. Such similarities were not present in the isotropic synthetic (FIGURE 20), thus providing other evidence of anisotropy in the thick lower shale. The use of the synthetic is a good way of getting a better understanding of the interpretation of the real data tomograms.

The string inversion version described above is based on an isotropic velocity model. Such a model does not account for angle dependent velocities. When anisotropy exists, in this case P-wave anisotropy, the resulting images exhibit distortions as discussed above. An estimate of the anisotropy provides useful information about the geology. Therefore it is of great importance to recognize the effects of anisotropy in the tomograms. Whereas, the string algorithm does not provide an anisotropic inversion, it can be used to analyze the variation of traveltime residual with angle, in this case launch angle of the rays. To test this hypothesis, we generated a 1-D string inversion from five iterations. Then we fixed the raypaths and ran one more iteration with restricted launch angles in five degree sectors from zero to forty-five degrees. The results of the 1-D backprojections is shown in FIGURE 26A along with an average of the limited angle images and the image obtained with the full +/-45 degree aperture (FIGURE 26B). (Note also that the color scale in Figure 23 is different.) I reiterate that these images are not inversions. Rather they are decompositions of the full aperture image into contributions from limited launch angles. What is evident is the fact that the thick shale layer below 2400 feet exhibits a large variation in velocity from over 15000 ft/s for launch angles near zero degrees to about 13000 ft/s near 45 degrees. The sonic log is less than 13000 ft/s in this zone. Other layers show variations too, but to much less degree. The layers immediately above and below 2250 feet show little or no variation with launch angle. (It would be more referred to use the local angle of the rays but the code is not implemented to output these values.) We see from Figure 23b that the average is remarkably similar to the full +/- 45 degree result.

So far we've only considered the anisotropic shale zone between 2500 and 2700 feet depth. It is also possible to come to a much more detailed model that, after inversion, closely resembles the real data tomogram. To come to such a model all available information has to be used. From well logs, mud reports, zero vertical offset velocities and a priori geological information, a 1-D model of the velocity structure between the wells can be constructed. FIGURE 27 shows this model for Newkirk. The gray colored areas are anisotropic. The synthetic traveltimes of this model were calculated for the correct real geometry, including the well deviation of the receiver borehole. After applying the same inversion procedures to both the synthetic data and the real data, the resulting tomograms are plotted in the FIGURE 28. The effect of simulating the actual survey geometry is visible in the shape of the low velocity feature in the lower left corner of the tomograms. The tomogram obtained from the synthetic data (FIGURE 28A) is a very good approximation of the real Newkirk data tomogram (FIGURE 28B). In addition, the model is consistent with the zero offset velocities, the well logs and the mud reports. In a way the model (Figure 27) can be seen not only as an interpretation of the crosswell tomogram, but also an inversion result.

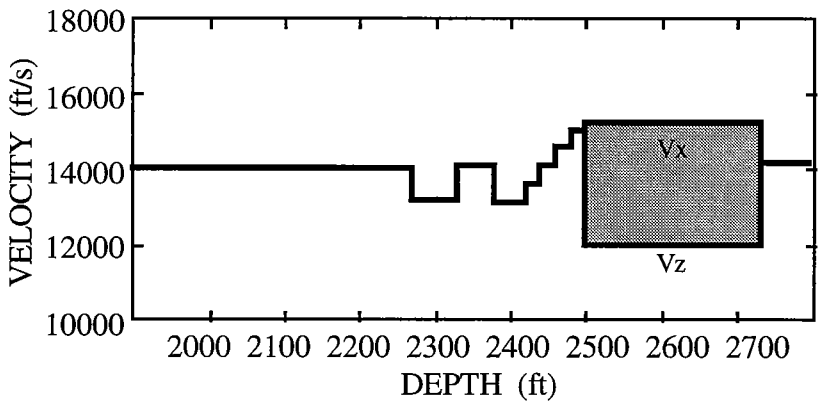

FIGURE 23. Isotropic synthetic velocity model with one anisotropic layer.

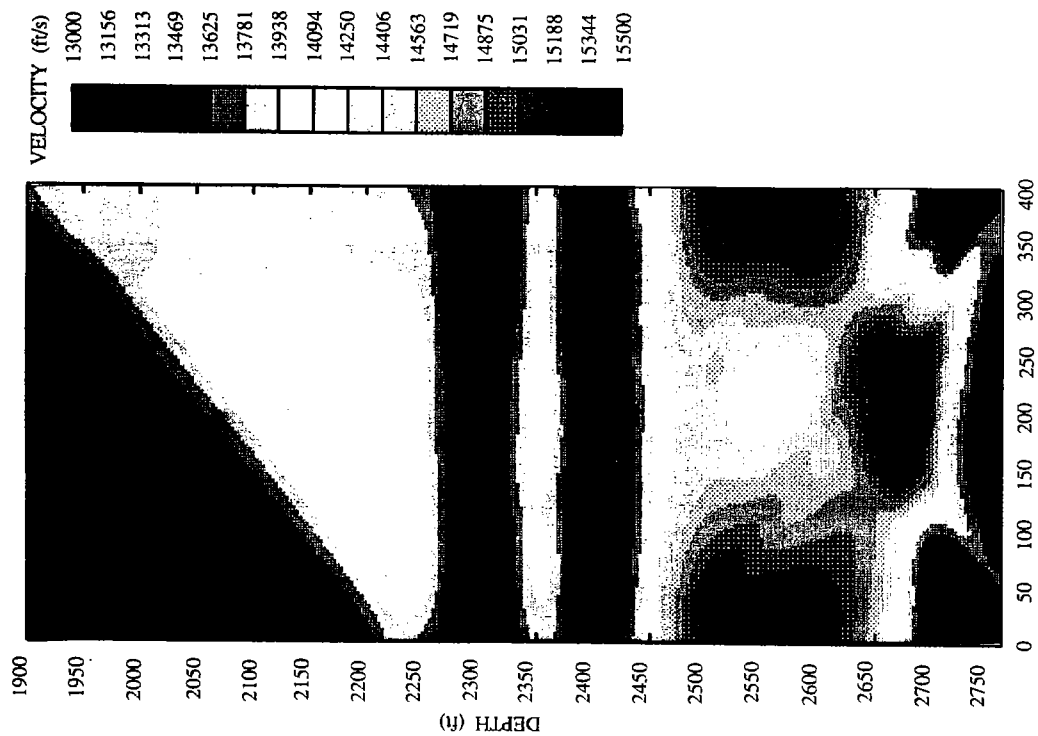

FIGURE 25. Crosswell tomogram: synthetic data (with missing traces) from anisotropic model.

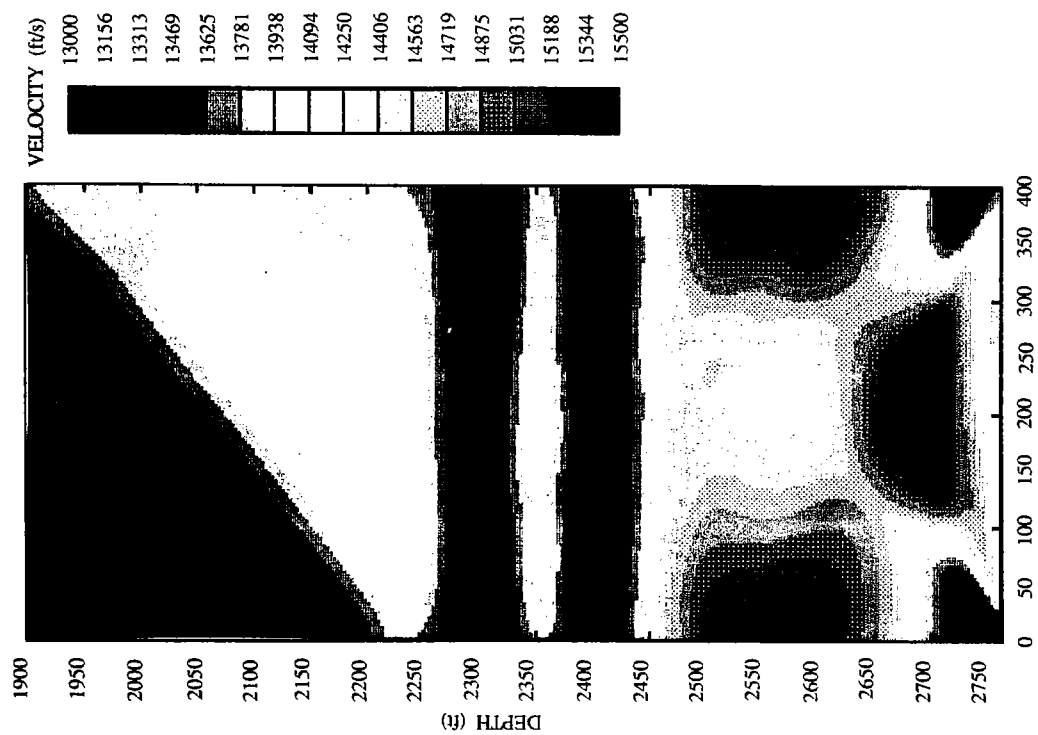

FIGURE 24. Crosswell tomogram: synthetic data from anisotropic model.

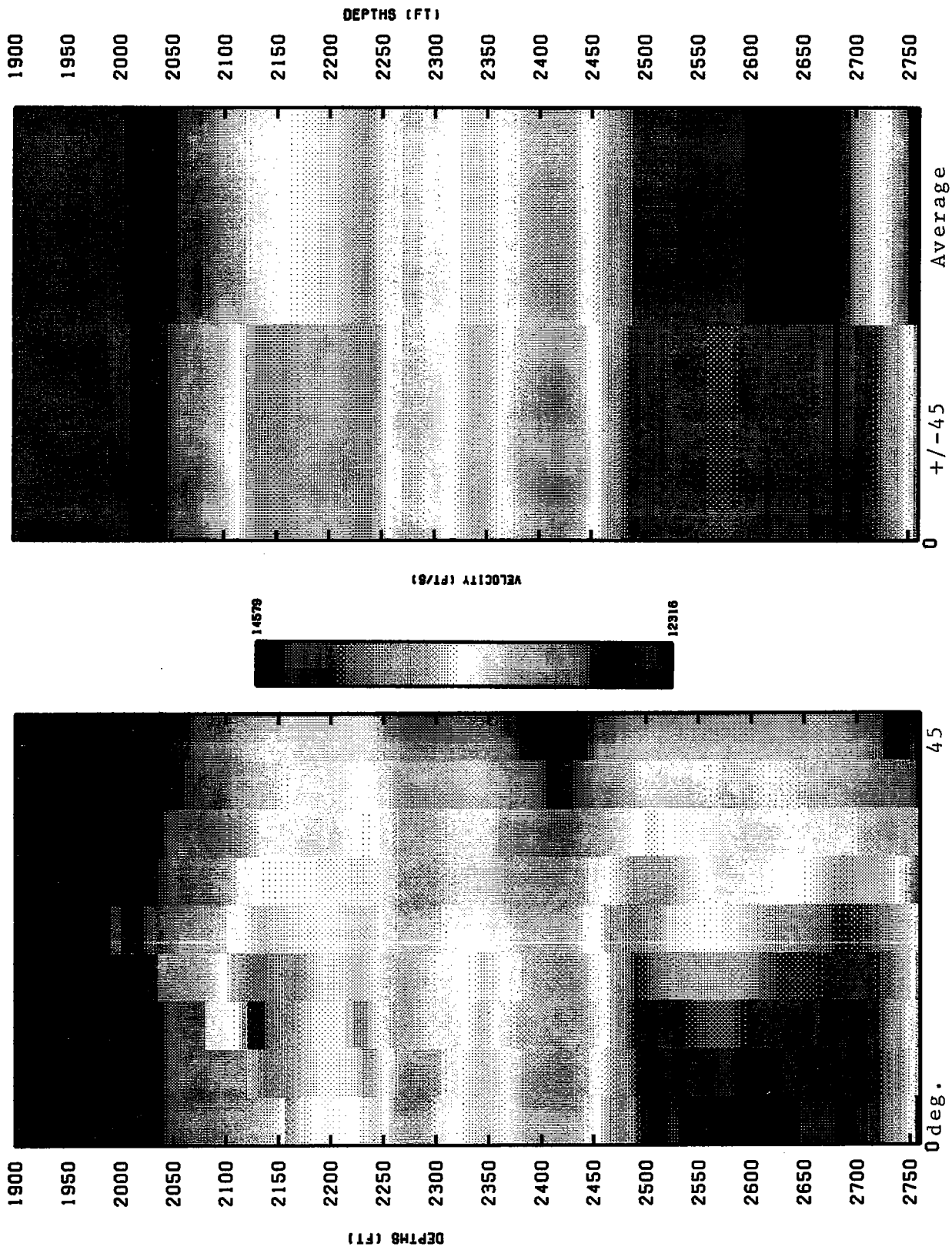

FIGURE 26. (a) Sequece of 1-D tomograms created from limited launch angles of 5 degrees from 0 to 45 degrees; (b) average of sequence (a) and full +/-45 degree inversion.

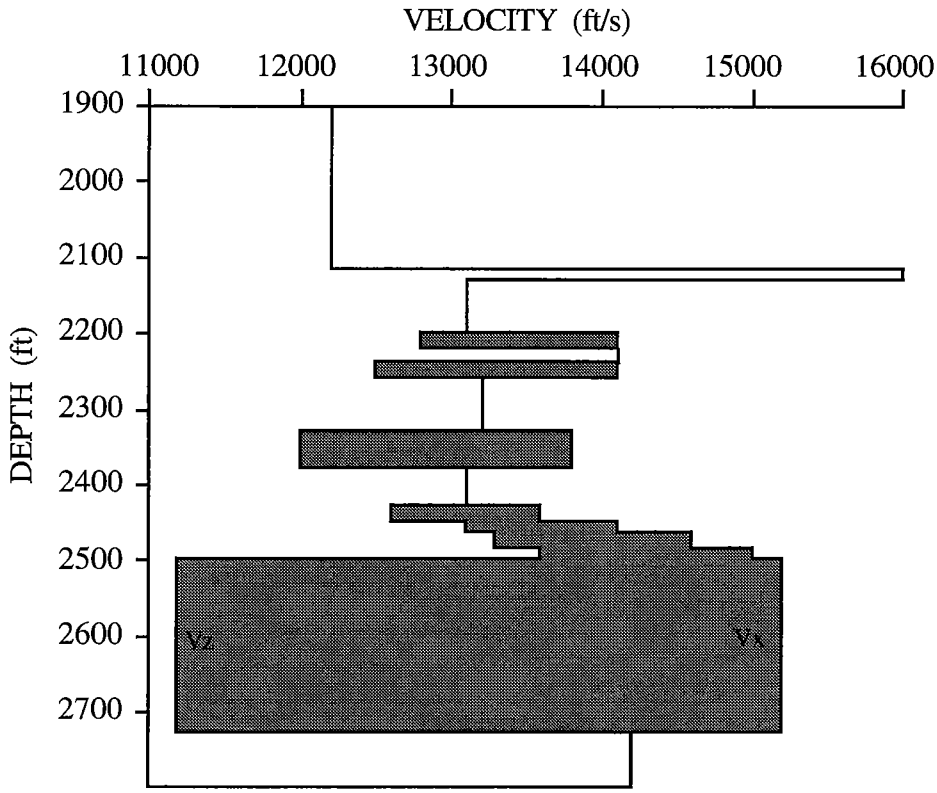

FIGURE 27. realistic anisotropic velocity model used for generating final synthetic data.

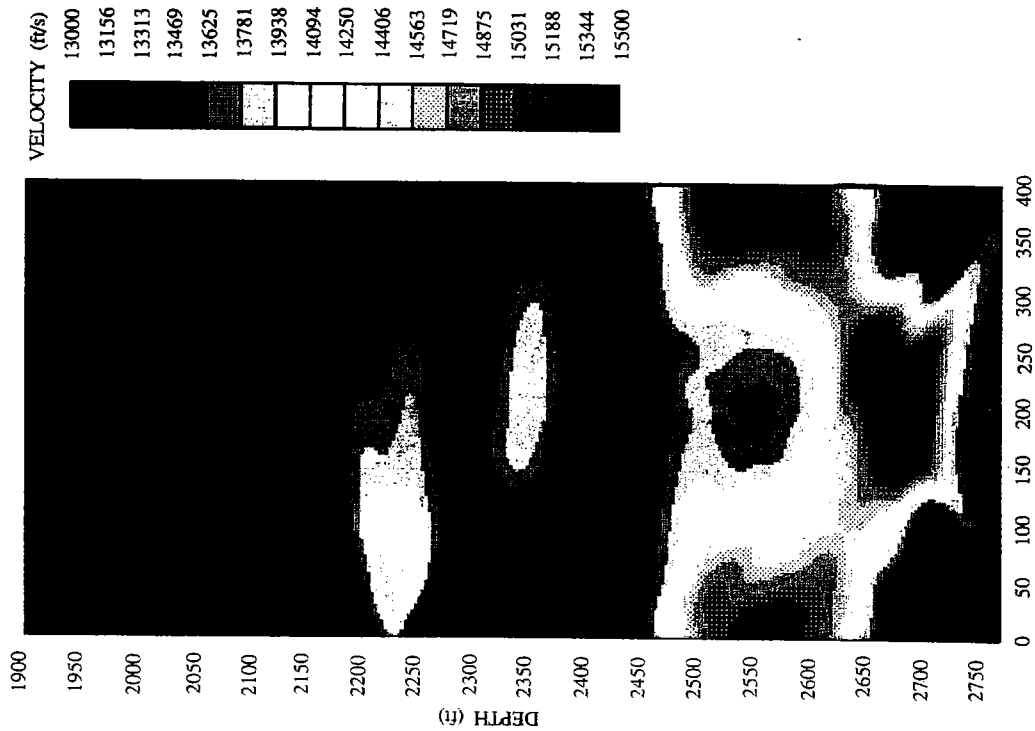

FIGURE 28B. Final crosswell tomogram: Newkirk field data.

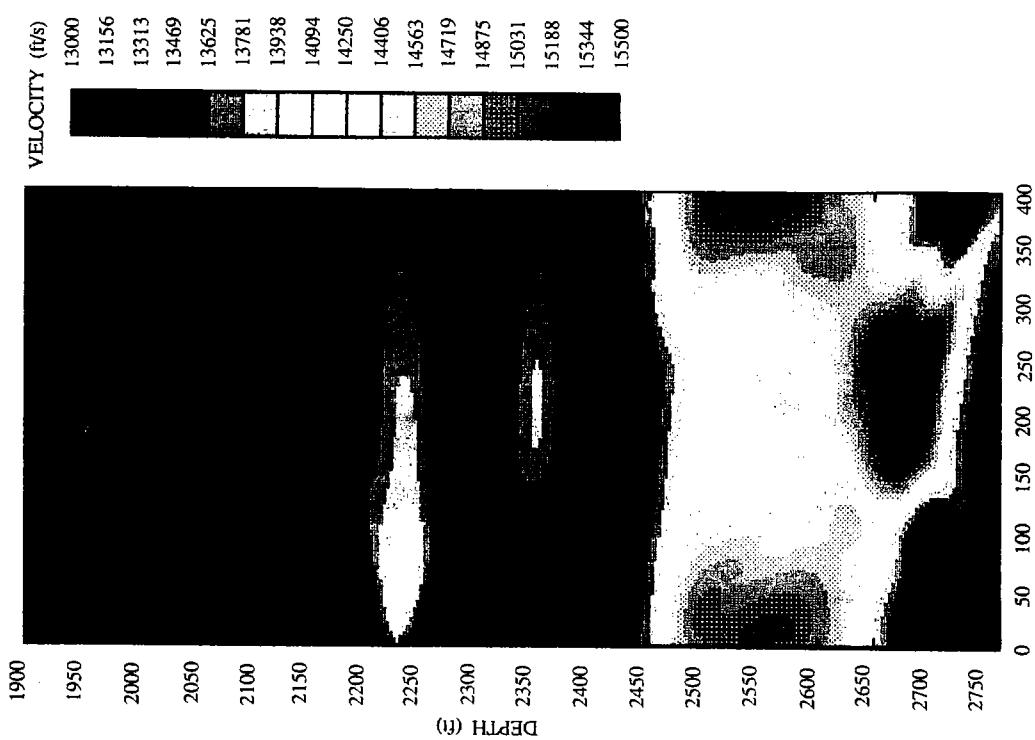

FIGURE 28A. Crosswell tomogram: synthetic data from realistic anisotropic model.

TRANSVERSE ISOTROPIC INVERSION

A better method of estimating the magnitude of the anisotropy is to describe the spatial and directional variations with a transverse isotropic forward and inverse model. We have chosen an elliptical model with variable axis of symmetry to describe the variations of velocity with directions and a layered structure (with straight interfaces of variable dip and intersect) to describe the variations with position (Michelena, et al, 1993). The data were inverted iteratively starting from a homogeneous isotropic model described by 130 horizontal layers. The axis of symmetry of this model was vertical. Ray bending at the interfaces is properly considered by tracing rays in the TI model. The starting values of slopes of the boundaries and axes of symmetry of the different layers didn't change significantly through the iterations and therefore, the final model also has horizontal layers with vertical axes of symmetry.

FIGURE 29A shows the estimated horizontal and vertical velocities with depth. Since the model for velocities is assumed to be elliptical, the estimated vertical velocity corresponds to the vertical velocity of a best fitting ellipse ($V_{z\text{-}nmo}$). FIGURE 29B shows a comparison of the horizontal velocity estimated from the crosswell data with the sonic log velocity. The log is blocked every 7 feet. Note the large anisotropy (25%) of the interval between 2500 feet and 2700 feet.

When comparing the estimated vertical velocity with the sonic log (FIGURE 29C) we see that the vertical component of estimated velocity is closer to the log than the horizontal velocity. Therefore, using an elliptical model for the velocities appears appropriate if we want to describe the data. Note, however, that the estimated vertical velocity is consistently less than or equal to to the log velocity, which means that the anisotropy is mostly non elliptical. In the interval between 2500 and 2700 feet $V_{z\text{-}nmo}$ alternates between being equal and lower than the log velocity which suggest that this interval may be combination of different layers whose anisotropy alternate between elliptical and non elliptical.

CONCLUSIONS

This study shows that P-wave anisotropy, missing data, and ray coverage have a great influence on the tomographic imaging. The artifacts associated with them completely overshadow other geometric information in the tomograms. Nevertheless, we have shown that in this sedimentary environment a model of the velocity distribution could be found with the use of the sonic - and zero vertical offset velocities, other well logs and geological information. Because the String inversion method is not suitable for imaging anisotropic media, the use of well logs and geological information is necessary to be able to interpret the inversion results. Tomograms derived from synthetic traveltimes compare remarkably well with the interpreted anisotropic model and the real Newkirk data. The isotropic results may be called an interpretative inversion.

A transverse isotropic inversion model does provide a consistent result for the crosswell and the log data, further supporting a model of P-wave anisotropy at the Newkirk site. The data were mathematically inverted for a 1-D anisotropic model with elliptical anisotropy. This inversion gave a much better match to the logs and a model consistent with the interpretative isotropic model. While this anisotropic inversion is a desirable improvement, it falls short in the area where the crosswell geometry is perceived to provide some advantages, namely in imaging lateral variations between wells.

REFERENCES

BREGMAN, N.D., BAILEY, R.C., and CHAPMAN, C.H., 1989, Cross-hole seismic tomography, Geophysics, **54**, 200-215.

HARRIS, J.M., MAVKO, G., MOOS, D., NOLEN-HOEKSEMA, R., 1990, Crosswell tomographic imaging of geological structures in Gulf coast sediments, STP volume **1**, No. 1, paper A.

HARRIS, J.M., 1991, Iterative Transform Tomography, STP volume **2**, No. 1, paper I.

HARRIS, J.M., 1992, Initial value raytracing in smoothly varying heterogeneous media, STP volume **3**, No. 1, paper I.

JUSTICE, J.H., VASSILIOU, A.A., SINGH, S., LOGEL, J.D., HANSEN, P.A., HALL, B.R., HETT, P.R., AND J.J SOLANKI, 1989, Acoustic tomography for enhanced oil recovery , The Leading Edge, **8**, **no.2**, 12 -19.

MICHELENA, REINALDO, Traveltime tomography in azimulthally Anisotropic media, STP volume **3**, No. 1, paper G.

QUEEN, J.H. and W.D. RIZER, 1990, Seismic Anisotropy and Natural Fractures, Journal of Geophysical Research , **95 - B7** , 11.255-11.273

WANG, G. AND J.M. HARRIS, 1992, Restoration of far offset cross-well traveltiems, STP volume **3**, No. 1, paper K.